A Comprehensive Numerical Study on Friction Reduction and Wear Resistance by Surface Coating on Cam/Tappet Pairs under Different Conditions

Bugao Lyu, Xianghui Meng *, Rui Zhang and Yi Cui

School of Mechanical Engineering, Shanghai Jiaotong University, Shanghai 200240, China;
bugaolv@sjtu.edu.cn (B.L.); zui972@sjtu.edu.cn (R.Z.); ycui@sjtu.edu.cn (Y.C.)
* Correspondence: xhmeng@sjtu.edu.cn

check for updates

Abstract: As a vital component in the valve train of internal combustion engines (ICEs), the cam/tappet pair undergoes high mechanical and thermal loads and usually works in a mixed and boundary lubrication regime. This leads to considerable friction loss and severe surface wear. Currently, the applications of diamond-like carbon (DLC) coatings for automotive components are becoming a promising strategy to reduce the friction and lower the wear. However, the practical performance of the coating is related to many factors, including friction coefficient, thermal properties, load conditions, and surface topography. In order to investigate these factors and successively improve the fuel efficiency and durability of the cam/tappet pair, a comprehensive multi-physics analytical model considering the mechanical, thermal and tribological properties of DLC coatings is established in this paper. Simulations are carried out for the coated as well as the uncoated cam/tappet conjunctions with different roughness at various ambient temperatures. The results show that both the fluid and asperity contact friction for the coated cam/tappet conjunction are significantly reduced due to their favourable characteristics. As a result, the friction loss of the coated cam/tappet pair is noticeably lower by almost 40% than that of the uncoated, despite a slightly higher asperity contact. In addition, the wear resistance of DLC coatings is also impressive, although the wear condition becomes progressively more severe with the increasing ambient temperature. Moreover, the roughness has complex effects on the friction and wear under different conditions.

Keywords: cam/tappet pair; surface coating; friction reduction; wear resistance; heavy load

1. Introduction

Mitigation of climate change has increasingly become a global consensus, in which reducing vehicle emissions and energy consumption is of great significance. According to the statistics, the transport of goods and people accounts for about 20% of the primary energy consumption and 23% of CO_2 emissions globally, of which more than 99.9% are powered by internal combustion engines (ICEs) [1]. With the extensive promotion of battery electric vehicles (BEVs), the market share of ICE vehicles is shrinking year by year. However, up to 2040, 75% of the automotive market will still rely upon the use of ICEs [2]. In addition, researchers have pointed out that blind elimination of ICEs may bring adverse effects, considering the harmful substances produced in the production and discard of batteries used in BEVs and the pollutant emissions caused by electricity generation [3]. Recently, a study demonstrated that the CO_2 emissions of a Tesla Class 3 during its lifetime with the German energy mix ranged from 11% to 28% more than the modern Diesel E6d Temp engines [4]. Therefore, the development of ICEs is still necessary to fight against global climate change. It is estimated that more than one-fifth of the fuel energy in passenger cars is used to overcome friction, of which about 15% is consumed in the valve

train [5]. As the core part of the valve train, the cam/tappet pair undergoes the highest loads in ICEs, and its friction loss accounts for about 85% of the whole valve train [6]. Hence, the study of thermal and tribological inefficiencies of the cam/tappet pair is imperative to improve upon fuel economy and its service life.

There have been a fair number of theoretical and experimental studies of the cam/tappet pair. Theoretical models are important tools for a better understanding of multi-physics tribodynamics of cam/tappet pairs. The fundamental work in the theoretical analysis may date back to Dowson et al. [7] in 1992, where the minimum oil film thickness of the whole cam cycle considering the influence of the squeeze film mechanism was analyzed by a numerical method and compared with the experimental results. However, it is known that the cam/tappet pair works in a mixed lubrication state. Thus, Chong et al. [8] used a mixed thermo-elastohydrodynamic lubrication (TEHL) model for the cam/tappet conjunction, while the frictional behaviour was conducted under the North American emission testing city cycle. The results demonstrated that under the low-speed emission cycles, the highest power losses occurred mainly when the lubricant film viscous shear was below the limiting Eyring shear stress. Recently, Torabi et al. [9] investigated the running-in behaviour of a cam-follower, and they pointed out that during the running-in period, the rate of flattening of surface roughness was a crucial factor. At the same time, experimental studies for cam/tappet pairs were conducted by researchers. To determine the friction loss of the cam/tappet pair in the whole valve train, Teodorescu et al. [10] conducted experiments where the friction losses of the cam/tappet, valve stem/valve guide, and sliding bearing of rocker shaft are separately measured. Green et al. [11] explored the wear condition of valve train in real engines with contaminated lubricating oil and obtained a group of wear data, which could be used in wear-prediction models.

To further improve the efficiency of the valve train, innovative technologies including new mechanical designs and surface modifications play a key role. Among these, surface coating using diamond-like carbon (DLC) by means of physical vapour deposition (PVD) and plasma-enhanced chemical vapour deposition (PECVD) are effective. High hardness, high resistance of wear and corrosion, chemical inertness, low friction characteristics, and thermal stability are factors that make DLC coatings the subject of many studies and seem suitable for use in engine parts [2], hard disk [12], and implantation of biomaterials [13]. The essential subclasses of DLC are hydrogenated amorphous carbon (a-C:H) and hydrogen free tetrahedral amorphous carbon (ta-C). Basically, a-C:H is an amorphous network composed of carbon and hydrogen, which consists of strongly cross-linked carbon atoms with mainly sp2 (graphitic-like) and sp3 (diamond-like) bonds, and its properties depend closely on the deposition process. More details about the properties and the deposition process of a-C:H can be found in the review article [14]. Another subclass, ta-C, are hydrogen free and are mostly (>80%) carbon, which is sp3 hybridized. The ta-C films are mainly produced from pure carbon targets by a filtered vacuum arc, as described in the review article [15]. DLC coatings deposited on the valve train components are already used in series productions, and investigations were carried out to understand the effects of DLC coatings in the valve train applications on friction reduction and anti-wear. Kano [16] in 2006 reported that super-low friction coefficients (below 0.01) in a cam and follower test-rig and friction reductions up to 45% in motor-driven valve train tests were observed while using ta-C coatings lubricated with the ester-containing PAO oil. Later, the influence of engine oil, additives, temperature, and camshaft speed on efficiency improvement using a-C:H:ZrC and a-C:H:X coatings was studied by Dobrenizki et al. [17]. Since the surface coatings can alter the tribological and thermal behaviour of contacts [18–20], Yu et al. [21] investigated the effects of mechanical and thermal coating properties on the cam/tappet contact under a TEHL model using numerical simulations. They pointed out that the friction reduction could be attributed to "the thermal barrier effect"—the coating serves as a thermal barrier increasing the contact temperature in the lubricating gap and therefore changing the shear resistance of the oil. Marian et al. [22] focused on the effect of DLC coatings with micro-texture. In their experiments, the solid and fluid friction force would be reduced in a wide range of lubrication regimes when using DLC-coatings, while micro-texturing may increase the fraction

of fluid friction. The formation of the transfer film between DLC coating and the counterpart is crucial to protect the surface from further wear and high friction [23–25]. In the experiments conducted by Gangopadhyay et al. [26], the results showed that in the presence of engine oil, the friction coefficient between the DLC-coated cam/tappet conjunction was slightly higher than that observed in the absence of the engine oil, despite significant wear resistance. Nevertheless, studies have proved the great potential for application on components under challenging lubricating and loading conditions.

For cam/tappet pairs, the real friction and wear performance of the DLC coating is influenced by many factors, including friction coefficient, thermal properties, load conditions, and surface topography. In order to investigate these factors to further improve the fuel efficiency and durability of the cam/tappet pair, a comprehensive multi-physics analytical model should be built. However, this kind of model has not been reported hitherto. Therefore, in this paper the mechanical, thermal and tribological properties of DLC coatings will be simultaneously incorporated in a comprehensive model, in which the lubrication, contact, wear, thermal and roughness effects will be considered together. Moreover, as modern engines undergo increasingly severe thermal and mechanical conditions, a much heavier load is inevitably encountered due to compact structure, abnormal combustion and dynamic conditions during the cam/tappet's service life. Therefore, the DLC coating's effect on cam/tappet pairs under heavy loads (compared to the normal load in a gasoline engine) will also be discussed.

2. Methodological Outline

A cam/tappet pair in the valve train from a gasoline engine of passenger cars is used in the current study. Figure 1 shows the schematic diagram of the cam/tappet pair, mainly including the cam, the tappet, the valve spring, and the valve shaft. The analysis comprises rigid-body dynamics and kinematics of the cam/tappet pair, a one-dimensional tribological model with appropriate rheological functions, and a thermal analysis considering the thermal barrier effect of the coatings. The friction and wear losses are evaluated to investigate the superiority of the DLC coating's reduction effect under different conditions, and the significance using DLC coatings applied in ICEs is emphasized.
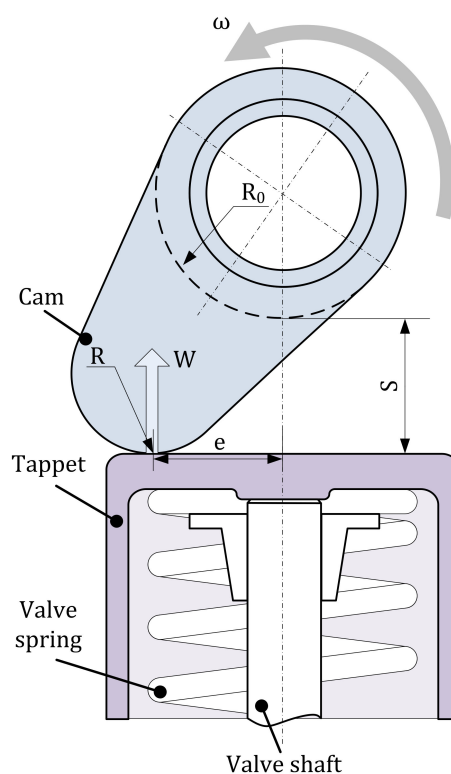

Figure 1. Schematic diagram of a cam/tappet pair in the valve train.

2.1. Kinematics and Dynamics

The sizes and parameters of the cam/tappet system are measured values for the real parts from a gasoline engine in this study, mainly including the cam, the tappet, the valve stem and the spring stiffness as well as its initial tension, which are listed in Table 1. Under the rotation speed of 2000 r/min for the crankshaft, the dynamics calculation is conducted in the commercial software ANSYS Workbench, where the inertia effect of the components is considered. The dynamics calculation yields the contact force between the cam and tappet and tappet displacement as well as its acceleration. The acceleration and displacement of the cam are to determine the entrainment velocity, the equivalent contact radius, and the velocities of the contact points on the cam and tappet, by using Equations (1) to (4) [21]:

$$j_\theta = \frac{1}{\omega^2}\frac{d^2s}{dt^2} \tag{1}$$

$$u_s = \omega(R_0 + s + 2j_\theta)/2 \tag{2}$$

$$R_C = R_0 + s + j_\theta \tag{3}$$

$$\begin{cases} u_a = \omega R_C \\ u_b = -\omega(R_0 + s - R_C) \end{cases} \tag{4}$$

where j_θ is the geometrical acceleration, u_s is the entrainment velocity, R_C is the equivalent contact radius, and u_a and u_b are the velocities of the contact points on the cam and tappet. Figure 2 shows the variations of the tappet displacement, the contact radius, the contact force, and the entrainment velocity from the valve opening angle of 0 to the closing angle of 164. The maximum tappet displacement is at the cam nose-to-tappet contact, where the cam angle is 80. The rise travel is the segment less than 80, while the return travel is the remainder. Note that there are two positions where the entrainment velocity is zero during the rise and return travels. Thus, the lubricant film may be extremely thin because of the absence of the entrainment effect and it will increase the risk of wear. The contact force between the cam and the tappet is mainly generated by the spring, and the maximum contact force can be observed near the cam nose region. However, the inertial force can be salient where the geometric acceleration is high. Therefore, there are two peaks on both sides of the cam nose caused by the high inertial force.
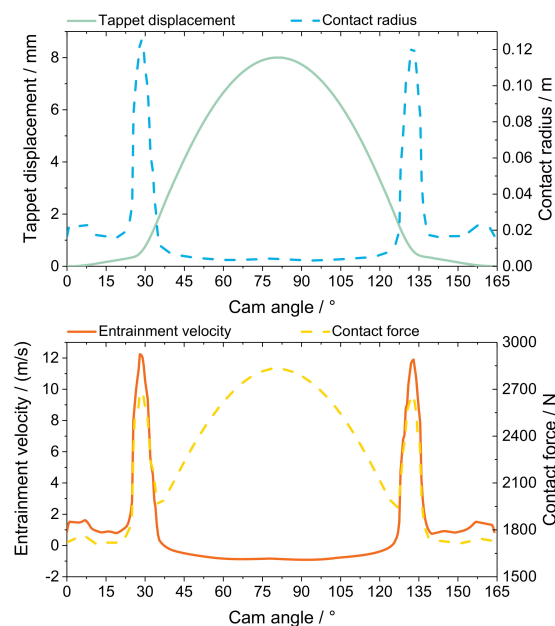

Figure 2. The kinematics and dynamics variations in a cam cycle for the tappet displacement, the contact radius, the entrainment velocity, and the contact force.

Table 1. Key parameters of the cam/tappet pair.

Base Circle Radius of Cam, mm	Maximum Lift of Cam, mm	Cam Depth, mm	Spring Stiffness, N/mm	Initial Tension of Spring, N
16.5	8.0041	12	16.6	172

2.2. Lubrication Analysis

The cam/tappet conjunction usually operates in mixed or even boundary lubrication state. Thus, the lubrication analysis in this section is crucial, as it will determine the probability of direct interaction of opposing surface asperities, which is believed to be the key factor initiating wear and scuffing. Considering the rheology relation of the lubricant and the elastic deformation of the contacting surfaces, the hydrodynamic pressure and film thickness distributions in the cam/tappet conjunction are described using a one-dimensional Reynolds equation.

2.2.1. Average Reynolds Equation

The cam/tappet conjunction can be simplified as one-dimensional line contact problem, where only the lubrication in the direction of cam rotation is considered. For the problem of mixed lubrication between rough surfaces, the following average transient Reynolds equation is introduced to describe the pressure distribution [27]:

$$\frac{\partial}{\partial x}\left(\phi_x \frac{\rho}{12\eta}h^3\frac{\partial p}{\partial x}\right) = u_s\left(\phi_c \frac{\partial(\rho h)}{\partial x} + \sigma\frac{\partial \phi_s}{\partial x}\right) + \phi_c\frac{\partial(\rho h)}{\partial t} \tag{5}$$

where x is the coordinate parallel to the cam rotation direction, t is the time, p is the lubricant film pressure, h is the film thickness, u_s is the entrainment velocity, σ is the composite roughness, and ρ and η are the lubricant's viscosity and density, which are affected by the film pressure and film temperature. ϕ_x, ϕ_c, ϕ_s are the pressure, contact, and shear flow factors, respectively, and they can be found in Patir and Cheng's work [27,28].

The Reynolds boundary condition is used to solve the partial differential equation above. The boundary conditions in the region of $x_s \leq x \leq x_e$ can be written as:

$$p|_{x=x_s} = 0; \; p|_{x=x_e} = 0; \; \frac{\partial p}{\partial x}|_{x=x_e} = 0 \tag{6}$$

where x_s and x_e represent the positions of the leading and trailing edges, respectively.

To solve Equation (5), the film thickness h is needed. Considering Hertzian geometry and the elastic deformation, the film thickness between the cam and tappet can be determined as:

$$h = h_0(t) + \frac{x^2}{2R} + v(x, t) \tag{7}$$

where h_0 is a constant value related to the applied load, $\frac{x^2}{2R}$ is the Hertzian geometry, v is the elastic deformation generated by the pressure between the contacting surfaces.

In fact, the film thickness and pressure are coupled through the Reynolds equation, which is an elliptic partial differential equation. On the one hand, the film pressure is determined from the Reynolds equation, and to solve the equation, the film thickness is required. On the other hand, the film thickness will be adjusted to reshape the pressure distribution to balance the applied load. When the film thickness is thin enough and is comparable to the surface roughness, asperity contact will occur. In this case (mixed lubrication), the applied load is partly supported by lubricant film and is partly supported by the asperities on the opposing rough surfaces. The process described above will be repeated in an iteration until the pressure is convergency and the load balance equation is satisfied.

The film thickness and pressure are both crucial to the friction calculation between the cam/tappet conjunction. Specifically, in mixed lubrication, the friction force comprises the film shear force and asperity contact friction. Regarding the film shear force, it is impacted both by the film thickness and

pressure. Generally, thinner film and higher pressure-gradient will result in larger film shear force and thus higher friction. As for the asperity contact friction, the film thickness or the gap between the contacting surfaces will directly determine the probability of interactions among opposing surface asperities. Thinner film will result in more severe asperity interaction and thus higher contact friction.

2.2.2. Rheology Relation

The lubricant rheological state which is susceptible to temperature and pressure has a significant effect on fluid lubrication. The Roelands viscosity-pressure-temperature equation is adopted to predict the viscosity variation [29]:

$$\eta = \eta_0 exp\left\{ (ln\eta_0 + 9.67)\left[\left(1 + 5.1 \times 10^{-9}p\right)^{0.68} \times \left(\frac{T - 138}{T_0 - 138}\right)^{-1.1} - 1 \right]\right\} \tag{8}$$

where η_0 is the initial lubricant viscosity, T is the lubricant temperature, and T_0 is the ambient temperature. The density of lubricant is also affected by the pressure and temperature [30]:

$$\rho = \rho_0\left[1 + \frac{0.6 \times 10^{-9}p}{1 + 1.7 \times 10^{-9}p} + D(T - T_0)\right] \tag{9}$$

where ρ_0 is the initial lubricant density, and $D = -0.00065K^{-1}$.

2.2.3. Elastic Deformation Calculation

The calculation method for the elastic deformation v is different, whether there is a coating layer or not. If there is no coating, a formula based on elastic half-space theory can be used to calculate the deformation of the isotropic substrate. The formula can be written as follows [21]:

$$v(x,t) = -\frac{2}{\pi E_{eq}} \int_{x_s}^{x_e} p(s,t) \ln(s - x)^2 ds \tag{10}$$

where E_{eq} is the equivalent Young's modulus. However, when there is a coating layer, which means the material is layered, v cannot be obtained in a straightforward manner aforementioned. In this study, a finite element model (FEM) is employed to calculate the elastic deformation of the coating and substrate. Based on the linear elastic theory [18], the elastic deformation of two contacting bodies can be replaced with an equivalent model in which one of the bodies is rigid, while the other is elastic. Furthermore, because the same substrate and coating materials are used for the cam and tappet, Habchi et al. [31] pointed out that the equivalent mechanical properties can be determined as follows:

$$\begin{cases} E_{s,\,eq} = \frac{E_s}{2}, \; v_{s,eq} = v_s \\ E_{c,\,eq} = \frac{E_c}{2}, \; v_{c,eq} = v_c \end{cases} \tag{11}$$

where E_s, E_c, v_s, and v_c are modulus of elasticity and Poisson's ratio for substrates and coatings, respectively. A cube with a side length 60 times that of the Hertzian half-contact width is sufficient to approximate a half-space in contact problems, as being demonstrated by Chu et al. [32]. Therefore, a square whose side length was 60 times the Hertzian half-contact width is used to approximate the substrate, and the geometry model shown in Figure 3 is the computation object to the FEM model. Considering the linear elasticity of the model, the elastic deformation of each point on the surface is contributed by the pressure of all other points, and the contribution of each point per unit pressure can be expressed by an influence coefficient, $D(x',x,t)$. The calculation can be stated as follows:

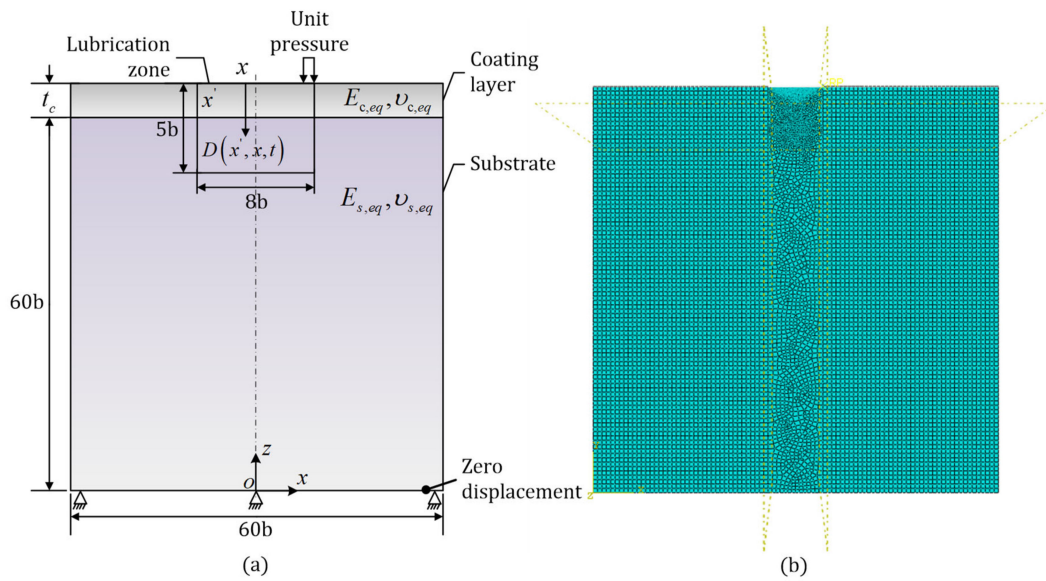$$v(x,t) = \sum_{x'=x_s}^{x_e} D(x',x,t)p(x',t) \tag{12}$$

Figure 3. The elastic deformation calculation: (**a**) the computation domain and boundary conditions and (**b**) the FEM model in ABAQUS.

Considering the symmetry of the model with respect to the contact center, it can be clearly concluded that $D(x', x, t) = D(-x', -x, t)$, then the influence coefficients of the whole lubrication area can be determined by applying unit pressure on the right lubrication area and outputting the elastic deformation of every discrete point. The calculation is conducted in the commercial FEM software ABAQUS. The elastic deformation calculation in this section is a plane strain problem, and the boundary conditions imposed on the FEM model are:

$$\begin{cases} (\sigma_2)_2 = 1 \left(i = 1, \text{ or } 2, \ldots, \text{ or } \frac{n+1}{2} \right) \text{ on the lubrication zone} \\ D_u = D_w = 0 \text{ on the bottom line} \\ \sigma_z = 0 \text{ elsewhere} \end{cases} \tag{13}$$

2.2.4. Load Balance Equation

The distributions of hydrodynamic pressure and asperity contact pressure is supposed to satisfy the load balance equation. It can be expressed as:

$$W(t) = \int_\Omega \left[p(x, t) + p_{asp}(x, t) \right] dx \tag{14}$$

where W is the applied load, and p_{asp} is the asperity contact pressure.

2.3. Asperity Contact Model

In mixed lubrication, the applied load is partly supported by the asperities on the opposing counter rough surfaces. The contact of rough surfaces is prevalent in engineering applications, and there are abundant models and approaches for the contact problem. Basically, there are statistical and deterministic models. The first statistical model for the rough surface contact dates back to the pioneering work of Greenwood and Williamson [33] (the GW model) in 1966. This classic model is based on the Hertz solution for a single elastic spherical asperity and is mainly suitable for pure elastic contacts. Other statistical models, like Greenwood and Tripp [34] (the GT model), Chang-Etsion-Bogythe [35] (the CEB model), and Kogut and Etsion [36] (the KE model), consider more contact patterns and surface parameters and, hence, provide more accurate results. Among these, the KE model presented by Kogut and Etsion in 2003 is a finite element based elastic-plastic model and

now widely used for the calculation of rough surface contact because of its convenience, high efficiency, and relatively accurate results. On the other hand, the deterministic approaches consider the real roughness distribution rather than several statistical parameters and, thus, are supposed to be more precise. Therefore, a deterministic approach based on the minimization of the total complementary potential energy principle proposed by Tian and Bhushan [37] is used to evaluate the contact state in this study. This deterministic approach utilizes the variational principle, which converted the two rough surfaces contact problem into quadratic programming in terms of solid contact pressure. Considering the real three-dimensional distribution of surface topography, the deterministic contact analysis will cost large computational overhead. However, with the fast Fourier transform (FFT) technique and several developed methodologies, such as the steepest descent method [38], Newton's method [37], and the Fletcher–Reeves version of the conjugate gradient method [39], the deterministic approach can be high efficiency and robust.

For the variational approach, the asperity contact pressure and the displacement can be obtained by solving an integral equation and minimizing the value of the equation, that is, minimizing the total complementary potential energy of the contact system. For a two-dimensional contact problem, the integral equation can be written as [38]:

$$\min_{H_s \geq p_c \geq 0} (f) = \min_{H_s \geq p_c \geq 0} \left(\frac{1}{2} \int_0^{l_1} \int_0^{l_2} p_c u \, dy_1 dy_2 + \int_0^{l_1} \int_0^{l_2} p_c \delta_c \, dy_1 dy_2 \right) \tag{15}$$

where y_1 and y_2 are the local coordinates of roughness, l_1 and l_2 are the roughness measurement length, u is the normal displacement, δ_c is the clearance between the undeformed surfaces, and p_c is the asperity contact pressure. The normal displacement u under a given contact pressure can be determined as [37]:

$$u(y_1, y_2) = \frac{1}{\pi E'} \int_{-\infty}^{+\infty} \int_{-\infty}^{+\infty} \frac{p_c(\xi, \varsigma)}{\sqrt{(y_1 - \xi)^2 + (y_2 - \varsigma)^2}} d\xi d\varsigma \tag{16}$$

Then the average contact pressure p_{asp} can be calculated as:

$$p_{asp} = \frac{\int_0^{l_1} \int_0^{l_2} p_c \, dy_1 dy_2}{l_1 l_2} \tag{17}$$

In this study, two surface topographies with different roughness are measured using a Keyence VK-X100/X200 3D laser-scanning confocal microscope (see Figure 4) and the parameters are listed in Table 2. A detailed analysis of the two measured surfaces can be found in Appendix A. The variations of the average contact pressure versus the separation of the contact surfaces using the KE model and the deterministic approach are shown in Figure 5. As can be seen that the calculation results using these two methods have similar tendencies. However, there are still some significant differences between them. Note that the roughness distribution is assumed as Gaussian distribution in the KE model, but the surface topography is not Gaussian in most cases. As a result, there are unneglectable limitations in the KE model, as shown in this section, and the maximum relative error is about 8.2%. Therefore, the deterministic results are adopted in this study.

Table 2. The roughness parameters for the two measured surfaces.

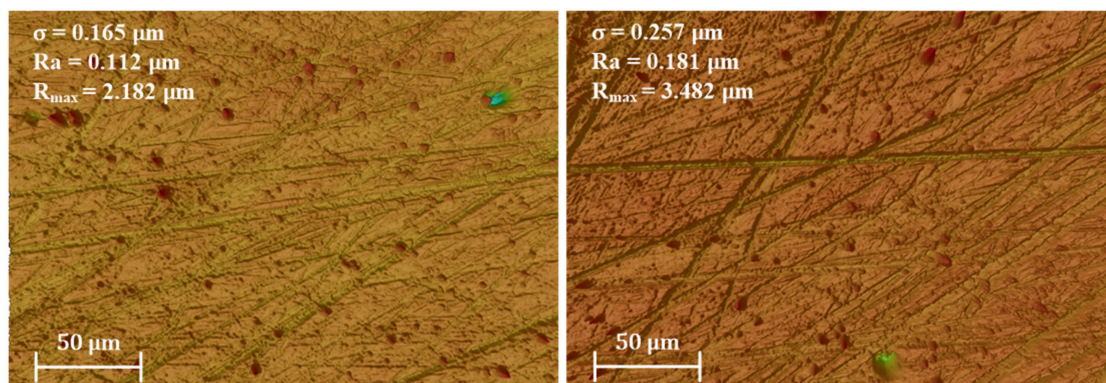| Parameter	Surface 1	Surface 2	Unit
Root mean square height, σ	0.165	0.2517	μm
Kurtosis, s_{ku}	10.6186	23.0696	-
Skewness, s_{sk}	2.5958	−1.0278	-
Density of asperities, η_α	0.4545	0.6224	μm^{-2}
Arithmetic mean asperity curvature, β	0.8521	0.4972	μm^{-1}

Figure 4. The two measured surface topographies with different roughness.
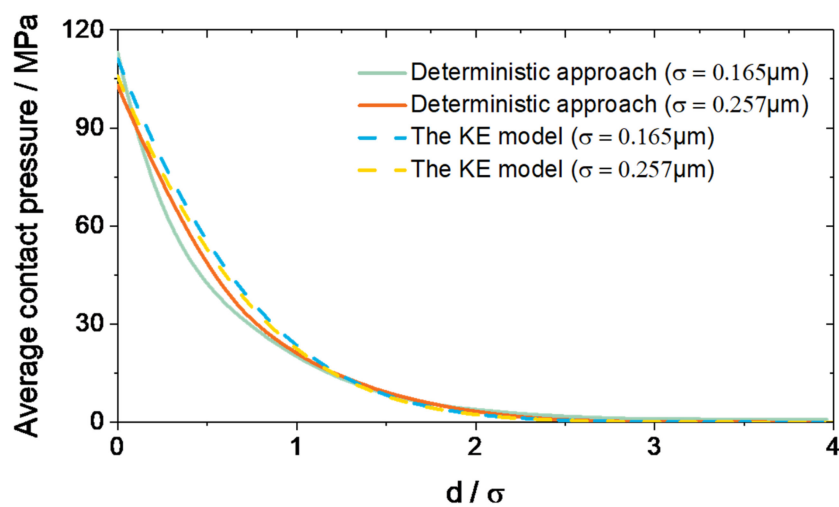

Figure 5. The variations of the average contact pressure versus the separation of the contact surfaces using the KE model and the deterministic approach.

2.4. Thermal Analysis

In the cam/tappet conjunction, the heat generated by viscous shear and compression of the lubricant as well as by the contact force of the asperities is partly carried away through lubricant convection and partly by conduction through the coatings and further transmitted to the substrates (see Figure 6). In this process, the temperature of the film will increase significantly, and successively affect the viscosity and density and then impact the pressure distribution of the lubricant film. It is a strong coupling relationship. In this paper, the energy equations are used to describe the aforementioned thermal process. The temperature distributions can be obtained by solving the energy equations of the lubricant film and the coatings as well as the substrates and simultaneously integrating the heat flux continuity equations of the lubricant–coating and coating– substrate interfaces.
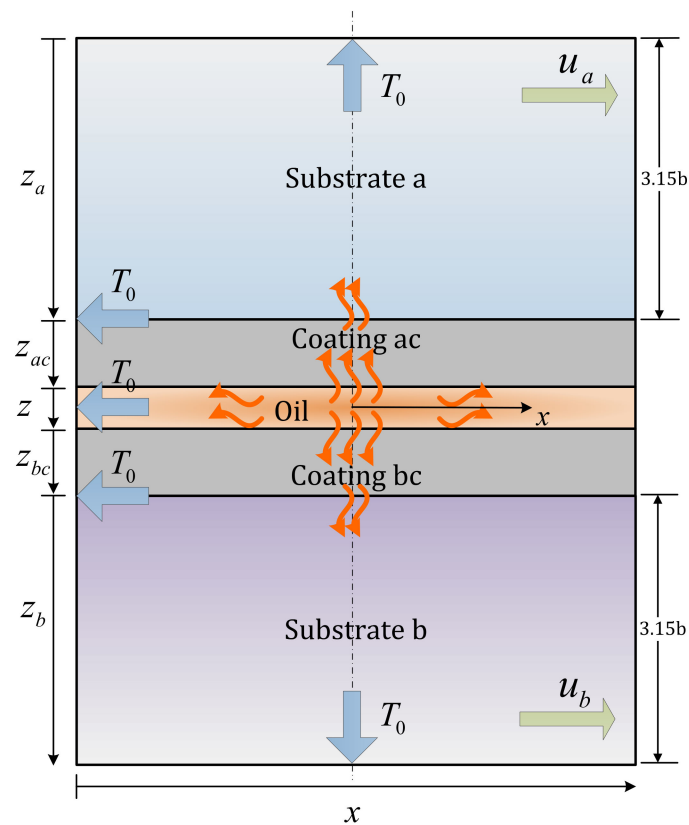
Figure 6. Schematics of the thermal model for the cam/tappet pair.

2.4.1. Lubricant Energy Equation

A two-dimensional energy equation is applied for the thermal analysis of the lubricant. Since the film is so thin between the contacting surfaces, it is assumed the heat convection in the film thickness direction (z direction) and the heat conduction in the moving direction (x direction) can be neglected [40]. It is noteworthy that in mix elastohydrodynamic lubrication, besides the viscous and compression heat of the lubricant, the contribution generated by asperity contact is considerable and should also be included in the energy equation [41]. After these simplifications and ignoring the heat radiation, the energy equation of the lubricant film can be written as:

$$c\left(\rho\frac{\partial T}{\partial t} + \rho u\frac{\partial T}{\partial x} - \rho w\frac{\partial T}{\partial z}\right) - k\frac{\partial^2 T}{\partial z^2} = \frac{T}{\rho}\frac{\partial \rho}{\partial T}\left(\frac{\partial p}{\partial t} + u\frac{\partial p}{\partial x}\right) + \eta\left(\frac{\partial u}{\partial z}\right)^2 + \frac{\mu_{asp}p_{asp}|u_a - u_b|}{h} \tag{18}$$

where c is the specific heat of the lubricant, k is the thermal conductivity of the lubricant, and u and w are the velocities of the control volumes in x and z directions, respectively. The left terms in the equation are the heat convection and heat conduction, and the right terms are the compression heat, viscous heat, and asperity contact heat, respectively.

Note that in the lubricant energy equation it is assumed the heat convection in film thickness direction (z direction) is neglected. This assumption is convincing when the film is rather thin. Fortunately, for most friction pairs operating under hydrodynamics lubrication, the lubrication film between contacting surfaces is in micro-scale or submicro-scale. Therefore, this assumption is valid for these friction pairs, including the cam/tappet pair.

To solve Equation (18), the velocities u and w are required, and they can be determined as follows:

$$
\begin{cases}
u = u_a + \frac{\partial P}{\partial x}\left(\int_0^z \frac{z}{\eta} dz - \frac{\int_0^h \frac{z}{\eta} dz}{\int_0^h \frac{1}{\eta} dz} \int_0^z \frac{dz}{\eta} \right) + \frac{u_b - u_a}{\int_0^h \frac{1}{\eta} dz} \int_0^z \frac{dz}{\eta} \\
w = -\frac{\partial}{\partial t}\left(\int_0^z \rho dz \right) - \frac{\partial}{\partial x}\left(\int_0^z \rho u dz \right)
\end{cases}
\tag{19}
$$

where u_a and u_b are the velocities of the cam and tappet, respectively.

2.4.2. Substrate and Coating Energy Equations

In the process of solving Equation (18), the surface temperature of the cam and tappet is crucial. As shown in Figure 6, in the cam/tappet conjunction, the heat is partly carried out by the flowing lubricant, whilst the rest is transferred by heat conduction through the contact surfaces. The heat conduction will affect the surface temperature, while the change of the surface temperature will also affect the lubricant temperature in turn. Based on the work of Yang et al. [40], the temperature of the coatings and substrates can be determined by the following equations:

$$
\begin{cases}
c_a \rho_a \left(\frac{\partial T}{\partial t} + u_a \frac{\partial T}{\partial x} \right) = k_a \frac{\partial^2 T}{\partial z_a^2} \\
c_{ac} \rho_{ac} \left(\frac{\partial T}{\partial t} + u_a \frac{\partial T}{\partial x} \right) = k_{ac} \frac{\partial^2 T}{\partial z_{ac}^2} \\
c_{bc} \rho_{bc} \left(\frac{\partial T}{\partial t} + u_b \frac{\partial T}{\partial x} \right) = k_{bc} \frac{\partial^2 T}{\partial z_{bc}^2} \\
c_b \rho_b \left(\frac{\partial T}{\partial t} + u_b \frac{\partial T}{\partial x} \right) = k_b \frac{\partial^2 T}{\partial z_b^2}
\end{cases}
\tag{20}
$$

where c, ρ, k are the specific heat capacity, density and thermal conductivity, and the subscripts a, b, ac, bc represent the substrates and coatings of the cam and tappet, respectively.

2.4.3. Heat Flux Continuity Equations

On the lubricant-coating and substrate-coating interfaces, the heat flux continuity equations must be satisfied. These equations can be expressed as follows:

$$
\begin{cases}
k_{ac} \frac{\partial T}{\partial z_{ac}}|_{z_{ac}=0} = k_a \frac{\partial T}{\partial z_a}|_{z_a=3.15b} \\
k_{ac} \frac{\partial T}{\partial z_{ac}}|_{z_{ac}=t_c} = k \frac{\partial T}{\partial z}|_{z=0} \\
k_{bc} \frac{\partial T}{\partial z_{bc}}|_{z_{bc}=0} = k \frac{\partial T}{\partial z}|_{z=h} \\
k_{bc} \frac{\partial T}{\partial z_{bc}}|_{z_{bc}=t_c} = k_b \frac{\partial T}{\partial z_b}|_{z_b=0}
\end{cases}
\tag{21}
$$

2.4.4. Boundary Conditions

Wang et al. [42] pointed out that a depth of 3.15 times the Hertzian half-contact width is sufficient to ensure a zero temperature gradient at the boundaries of the substrates, as shown in Figure 6. It should be noted that when $u_b < 0$, the boundary conditions on the surfaces in the leading and trailing regions will be reversed:

$$\begin{cases} T(x, z_a, t)|x = x_s = T_0 \\ T(x, z_{ac}, t)|x = x_s = T_0 \\ T(x, z_b, t)|x = x_s = T_0, \ u_b \geq 0 \\ T(x, z_{bc}, t)|x = x_s = T_0, \ u_b \geq 0 \\ T(x, z_b, t)|x = x_e = T_0, \ u_b < 0 \\ T(x, z_{bc}, t)|x = x_e = T_0, \ u_b < 0 \\ T(x, z_a, t)|z_a = 0 = T_0 \\ T(x, z_b, t)|z_b = 3.15 b_{max} = T_0 \end{cases} \tag{22}$$

2.5. Friction Loss and Wear Evaluation

In the mixed lubrication, the total friction is the superposition of the lubricant viscous friction and the asperity contact friction:

$$f = f_{visco} + f_{asp} \tag{23}$$

where f, f_{visco} and f_{asp} are the total friction, the lubricant viscous friction, and the asperity contact friction, respectively. In the flowing fluid, the shear force and friction force due to the viscosity can be calculated as follows [38]:

$$\begin{cases} \tau = \left(\phi_f + \phi_{fs} \right) \frac{\eta(u_a - u_b)}{h} + \phi_{fp} \frac{h}{2} \frac{\partial p}{\partial x} \\ f_{visco} = L \int_{x_s}^{x_e} \tau dx \end{cases} \tag{24}$$

where τ is the shear force, L is the cam thickness, and ϕ_f, ϕ_{fs}, as well as ϕ_{fp} are the flow factors which can be found in Patir and Cheng's work [28]. Note that Eyring shear stress, τ_0, determines the shear threshold for non-Newtonian behaviour of the lubricant. Moreover, the friction due to the interacting asperities can be determined as:

$$f_{asp} = L \int_{x_s}^{x_e} \mu_{asp} p_{asp} dx \tag{25}$$

where μ_{asp} is the friction coefficient of the dry contact surface. Note that the friction coefficients of the coated surface and uncoated surface are quite different. The friction coefficient of the DLC-coated surface is lower than 0.1 [24,43]. Consequently, the friction work W_f in mixed lubrication can be written as follows:

$$W_f = \int_0^T f|u_a - u_b|dt \tag{26}$$

Surface wear is mainly affected by the material properties of the friction pair and the working conditions of the tribology system. Researchers have proposed a large number of theoretical and empirical models on wear to reveal the relationship between wear and internal as well as external factors [44,45]. Among these models, the Archard wear model is widely accepted, and it is considered to be simple but also reasonable.

According to the Archard model, the wear depth is related to the normal load, the sliding distance, and the material hardness. In mixed lubrication, the normal load is sharing both by the lubricant film and the contacting asperities. Surface wear will merely emerge in the asperity contact region, and, thus, the Archard model can be written as follows [45]:

$$h_{wear} = K_W \frac{p_{asp}}{H} S \tag{27}$$

where h_{wear} is the wear depth, p_{asp} is the asperity load, H is the material hardness, S is the slide distance, and K_W is the wear coefficient, which is essential for wear calculation and can be found in wear

experiments [25,46]. Because the wear process is transient, using Equation (28), the wear depth at each time step can be rewritten as follows:

$$\Delta h_{wear} = K_W \frac{p_{asp}}{H} \Delta S \tag{28}$$

Therefore, the current wear depth can be estimated by accumulating the wear of every step before.

The wear coefficient is thought to be constant in the whole running process [45]. However, it may vary with the operating conditions [44,45]. Nevertheless, the present paper puts a greater focus on the comparison between the coated and uncoated cam/tappet pairs on friction reduction and wear resistance. It is sufficient to show the priority of DLC coatings on wear resistance under the same operation condition.

3. Results and Discussion

The coating in Reference [20] is an industrial hydrogen containing DLC coating (a-C:H) widely applied in gasoline engines and it is deposited on the substrate by means of plasma enhanced chemical vapour deposition (PECVD). The mechanical and thermal properties of the coating in Reference [20] and the substrates which are standard uncoated cam and tappet from the gasoline engine are listed in Table 3. Table 4 provides the rheological properties of the lubricant at the reference temperatures, and the effective density and viscosity values are predicted at the operating temperatures and pressures using Equations (7) and (8).

Table 3. The mechanical/thermal properties of substrate material and the coating layer.

Parameters	Value	Unit
Young's modulus of substrates, E_s	210	GPa
Poisson ratio of substrates, v_s	0.3	-
Young's modulus of coatings, E_c	305	GPa
Poisson ratio of coatings, v_c	0.3	-
Coating thickness, t_c	4	μm
Density of substrates, $\rho_{a,b}$	7850	Kg/m^3
Density of coatings, ρ_c	3500	Kg/m^3
Specific heat of substrates, $c_{a,b}$	470	J/(kg·K)
Specific heat of coatings, $c_{ac,bc}$	200	J/(kg·K)
Thermal conductivity of substrates, $k_{a,b}$	46	W/(m·K)
Thermal conductivity of coatings, $k_{ac,bc}$	5	W/(m·K)

Table 4. The lubricant rheological parameters.

Parameters	Value	Unit
Viscosity of lubricant at 313 K, η_0	0.01	Pa·s
Density of lubricant at 313 K, ρ_0	875	Kg/m^3
Specific heat of lubricant, c	2000	J/(kg·K)
Thermal conductivity of lubricant, k	0.14	W/(m·K)
Thermal expansion coefficient, α	6.5×10^{-4}	K^{-1}

To study the DLC coatings' reduction effect under different conditions, the simulations are carried out at various ambient temperatures. Different ambient temperatures from 40 C to 100 C correspond to different engine operation stages. A lower temperature corresponds to the engine at the starting phase, while a higher temperature may represent the steady state stage. Moreover, the DLC coatings' effect under a much heavier-load condition whose contact force is 10 times the normal load shown in Figure 2 is discussed in this paper. The methodology adapted in this study has already been validated in [18,21,22].

3.1. Normal-Load Conditions

At the operating temperature of 40 C, the lubrication state of the cam/tappet pair changes dramatically in a cam cycle and is closely related to whether there is a coating layer and its surface roughness. Figure 7 shows the predicted variations with cam angle for the minimum film thickness, the maximum film pressure, the maximum temperature of the lubricant, and the asperity contact area ratio in the cam/tappet conjunction. It can be seen that the curve of film thickness (Figure 7a) has the same tendency with that of entrainment velocity (Figure 2), where the minimum values are located at the cam angles of 37.5 and 124.5 corresponding to the zero entrainment velocity positions. The film thickness is comparable to the asperity heights during the cam cycle, and consequently, a mixed regime of lubrication is dominant. The film pressure variations are shown in Figure 8b, and the trend of which is basically determined by the contact force (Figure 2). The maximum hydrodynamic pressure is larger than 0.4 GPa, which will generate considerable surface deformation and high friction. The film temperature (Figure 7c) shows analogous variations with the hydrodynamic pressure, especially in the cam nose region. In addition, the variations of the asperity contact area ratio (Figure 7d) demonstrate that the cam/tappet conjunction runs mainly under mixed and even boundary lubrication state and the asperity contact ratio may exceed 5%. It can be seen that the asperity contact is directly related to the entrainment velocity. Lower entrainment velocity results in thinner film and thus a more severe asperity contact. Among these results above, the most significant effect of DLC coatings is on lubricant temperature. The results with DLC coatings show higher film temperature due to the 'low thermal inertia' characteristic defined by Habchi et al. [18], which means the DLC coating layer can effectively insulate the heat transfer from the film and serve as a thermal barrier and thus leading to higher film temperature. Subsequently, the film thickness with DLC coatings is slightly thinner because of the higher temperature and its thermal film shear thinning effect. However, in the mixed lubrication with such a thin film thickness, the lubricant film shear thinning with temperature is marginal and the difference between the coated and uncoated surfaces in film thickness is quite small. The mechanical characteristics of the coating layer can alter the hydrodynamic pressure, as shown in Figure 7b. According to Habchi et al. [18] as well as Yu et al. [21], because of the high elastic modulus of DLC coatings, for the same load, the surface elastic deformation will be lower, which will reduce the film thickness, and successively increase the oil film pressure. The impact of surface roughness is mainly reflected on the asperity contact ratio, as shown in Figure 7d. In the cases with larger roughness, there are more asperities in contact, thus the applied load is more borne by asperities. It will decrease the film bearing ratio, and the hydrodynamic pressure will also be lower accordingly.

The anti-friction effect of coatings on friction pairs by altering the tribological and thermal behaviour of contacts is mainly reflected in two aspects. On the one hand, according to Hauert [23] and Kim et al. [43], the friction coefficient of the DLC-coated surface is lower than that of the uncoated, and the transfer layer formed between the interacting surfaces can greatly reduce the solid friction. On the other hand, the thermal properties of DLC coatings make them perform a favourable thermal isolation characteristic. The heat transfer from the film to the contiguous contacting surfaces is hindered, thus the temperature of the film is significantly higher than that of the uncoated, leading to lower lubricant viscosity and shear force. More detailed explanations can be found in the literature [19,20]. Figure 8 shows the predicted variations with cam angle for the asperity contact friction, the fluid friction, and the total friction in the cam/tappet conjunction. The variation of asperity friction in Figure 8a is in line with the asperity contact ratio (Figure 7d). Although lubricant film shear thinning with temperature exacerbates asperity friction, the asperity friction with DLC coatings is still much lower than that without coatings due to their desirable friction coefficient. In addition, surfaces with higher roughness result in larger contact ratio and thus more considerable asperity contact friction. The gap between coated and uncoated surfaces in fluid friction shown in Figure 8b can be attributed to the aforementioned 'thermal barrier effect', while in contrast to the asperity friction, the fluid friction decreases with surface roughness. This is because the hydrodynamic pressure is weakened when the surface roughness is larger (as shown in Figure 7b). Figure 8c shows the combined effects of viscous

and asperity friction contributions during a cam cycle. Overall, the total friction for DLC-coated surfaces is significantly lower than that for uncoated surfaces, and as the asperity contact dominates the friction in cam tappet conjunctions under the normal load, the total friction will increase with surface roughness.
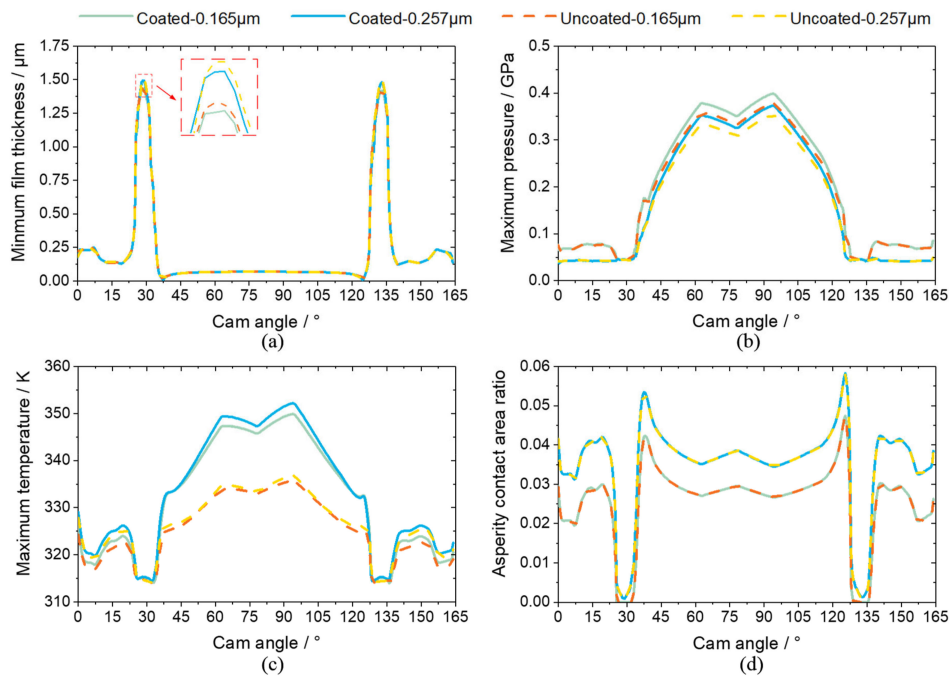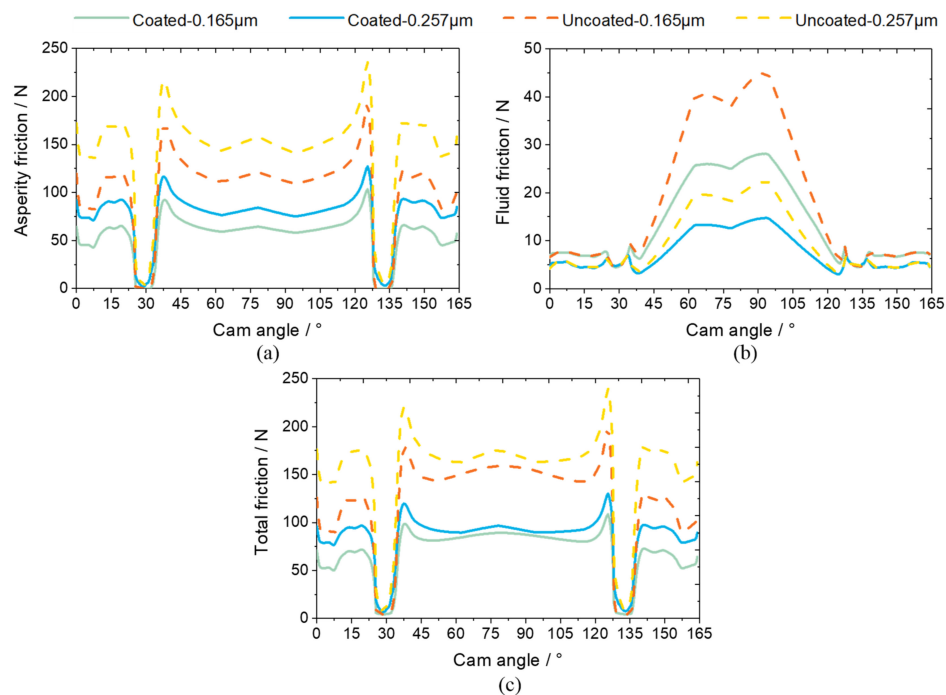

Figure 7. Variations of the lubrication state during a cam cycle under the normal load: (**a**) the minimum film thickness, (**b**) the maximum film pressure, (**c**) the maximum temperature of the lubricant, and (**d**) the asperity contact area ratio.

Figure 8. Frictional variations during a cam cycle under the normal load: (**a**) asperity contact friction, (**b**) fluid friction, and (**c**) total friction.

Figure 9 shows the friction works in the cam/tappet conjunction with different surface conditions at various ambient temperatures during a cam cycle, comprising the consumption of fluid friction and asperity contact friction. It can be seen that the friction work for each surface condition is consistent with the total friction force (shown in Figure 8c), specifically, the friction work for the coated surface is significantly reduced by about 40%, compared with that for the uncoated. Asperity friction consumes the majority of the total friction loss in these cases, which continuously increases in transition from medium to high ambient temperature phase. During the extra high-temperature phase, asperity interactions are at their most severe state, leading to the highest friction work. This can be attributed to the formation of slightly thinner lubricant film, exacerbating the extent of asperity interactions. Regarding the friction work consumed by fluid friction, it reduces with ambient temperature due to the decreasing lubricant viscosity. At the ambient temperature of 100 C, the fluid friction loss merely accounts for a minor part of the total work. Similar results are shown in the experiments conducted by Dobrenizki et al. [17].
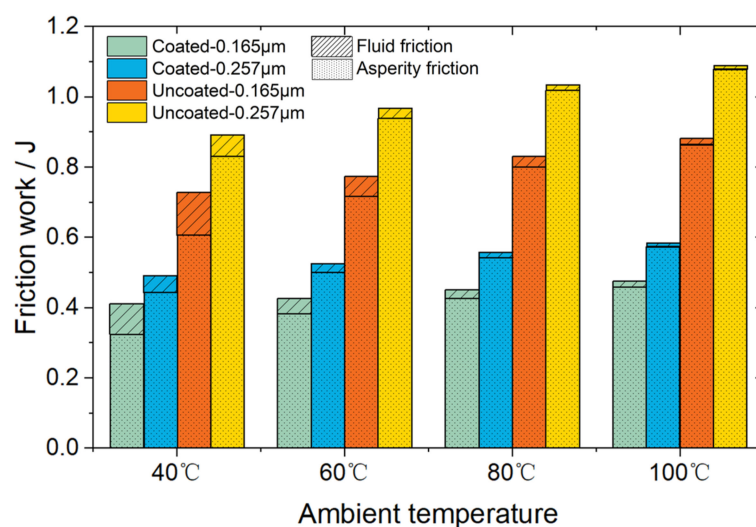

Figure 9. The friction work for different surface conditions at various ambient temperatures in a cam cycle under the normal load.

DLC coatings display prominent superiority in wear resistance in the cam/tappet conjunction. As shown in Figure 10, the wear volume of coated surfaces is far less than that of uncoated surfaces, despite a higher asperity contact shown in Figure 7d. According to the Archard wear model, this can be mainly attributed to DLC coatings' high hardness and low wear coefficient. The transfer layer formed between the DLC coating and the counterpart can protect the surface from further wear, as demonstrated in the literature [23–25]. Besides, DLC has been shown to effectively improve the wear performance of high-pressure elastohydrodynamic contacts by preventing the high stresses from penetrating into the substrate material [47]. Surface wear is directly related to the asperity contact pressure. As a consequence, in cases with higher roughness, the wear condition is more severe. It is noteworthy that with the increase of the ambient temperature, the surface wear becomes increasingly severe, which is due to the increasing asperity contact and the weakening bear capacity of the lubricant.
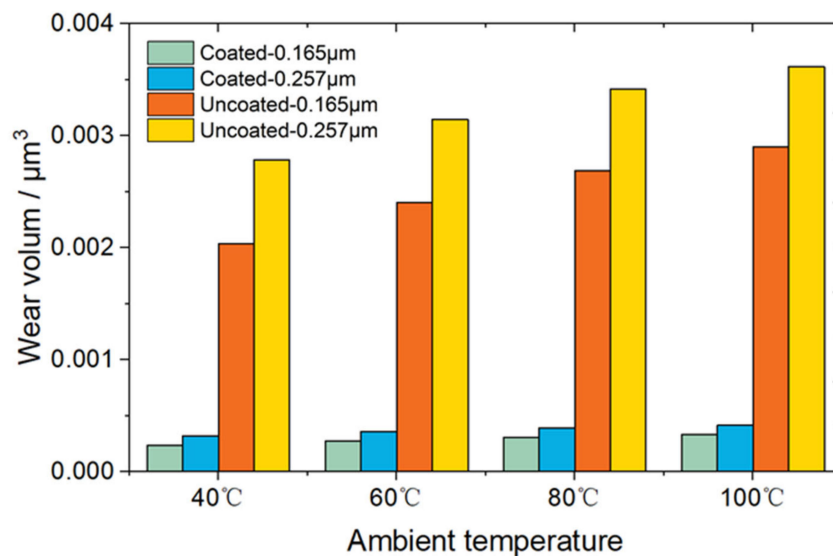
Figure 10. The wear volume for different surface conditions at various ambient temperatures in a cam cycle under the normal load.

3.2. Heavy-Load Conditions

As modern engines undergo increasingly severe thermal and mechanical conditions, a much heavier load is inevitably encountered due to the compact structure, abnormal combustion and dynamic conditions during running. Figure 11 shows the predicted variations with cam angle for the minimum film thickness, the maximum film pressure, the maximum temperature of the lubricant, and the asperity contact area ratio under heavy-load conditions. Compared with the normal load in the last section, the results for the heavy load show a similar variation trend, but their numerical values have changed substantially. Owing to the much heavier load, the lubricant film is further squeezed and becomes thinner, and the minimum film thickness in the cam nose region shown in Figure 11a is lower than 40 nm. Correspondingly, Figure 11b shows that the maximum hydrodynamic pressure may exceed 1.8 GPa, which will bring dramatic pressure-viscosity effect and result in a sharp increase in lubricant viscosity. However, under such high pressure, more friction heat will be generated, leading to a higher lubricant temperature, and the maximum oil film temperature may reach 540 k (shown in Figure 11c). It will also bring strong temperature-viscosity effect and cause a significant decrease in the lubricant viscosity. The lubricant viscosity is both susceptible to the pressure and temperature in a highly nonlinear way (Equation (7)), and the viscosity distribution in a whole cam cycle will be demonstrated and discussed in detail below. In addition, the asperity contact ratio is also higher due to the thinner film thickness (Figure 11d).

According to the frictional variation with cam angle under the heavy load (shown in Figure 12), both the fluid friction and asperity friction are greatly increased, among which the increase of fluid friction is quite noticeable. Under the heavy load, the results of these two frictions for the coated surface are significantly lower than those for the uncoated surface, indicating that the anti-friction effect of DLC coatings is still valid. Interestingly, by contrast with the cases in the last section, the maximum fluid friction under the much heavier load emerges in the vicinity of cam angle of 37.5, and it is much larger than that in the cam nose region. It can be seen from Equation (25) that the viscosity is essential for the fluid friction calculation. While the viscosity itself is affected by the non-linear effect of pressure and temperature simultaneously, which shows a comprehensive relationship. Therefore, it is necessary to investigate the lubricant viscosity variation during a whole cam cycle. Figure 13 manifests the distributions of the lubricant viscosity in *x*-direction from −2 to 2 during a whole cam cycle for each surface condition at various ambient temperatures. The high viscosity region is mainly concentrated in the Hertz contact region (from −1 to 1 in *x*-direction), and the variation of viscosity

in a cam cycle is in line with the fluid friction. Specifically, the highest viscosity also appears near the cam angle of 37.5 and is much larger than that in the cam nose region. Considering the variations of pressure and temperature in Figure 11, although the hydrodynamic pressure in the cam nose region is larger than others, leading to a significant pressure-viscosity effect. The lubricant temperature in this region is also the highest, which initiates a strong thermal effect and reduces the lubricant viscosity successively. However, near the cam angle of 37.5, the hydrodynamic pressure is relatively high accompanying a mild lubricant temperature, resulting in the highest lubricant viscosity, which exceeds 4 Pa·s. Therefore, under the combined pressure-temperature-viscosity effect in a highly non-linear way, the viscosity distribution in Figure 14 is obtained. On the other hand, with the increase of the ambient temperature, the temperature-viscosity effect near the cam angle of 37.5 is gradually dominant. As the lubricant viscosity declines rapidly, the viscosity near the cam angle of 37.5 is increasingly close to that in the cam nose region. Overall, the variation of the fluid friction in a cam cycle is highly consistent with its viscosity, and under the non-linear effect among pressure, temperature, and viscosity, it presents a complex pattern. In addition, the lubricant viscosity for the coated surface is significantly lower than that for the uncoated due to its higher temperature, which also reveals the mechanism of the DLC coating's reduction effect on fluid friction, as demonstrated in the literature [19,20].
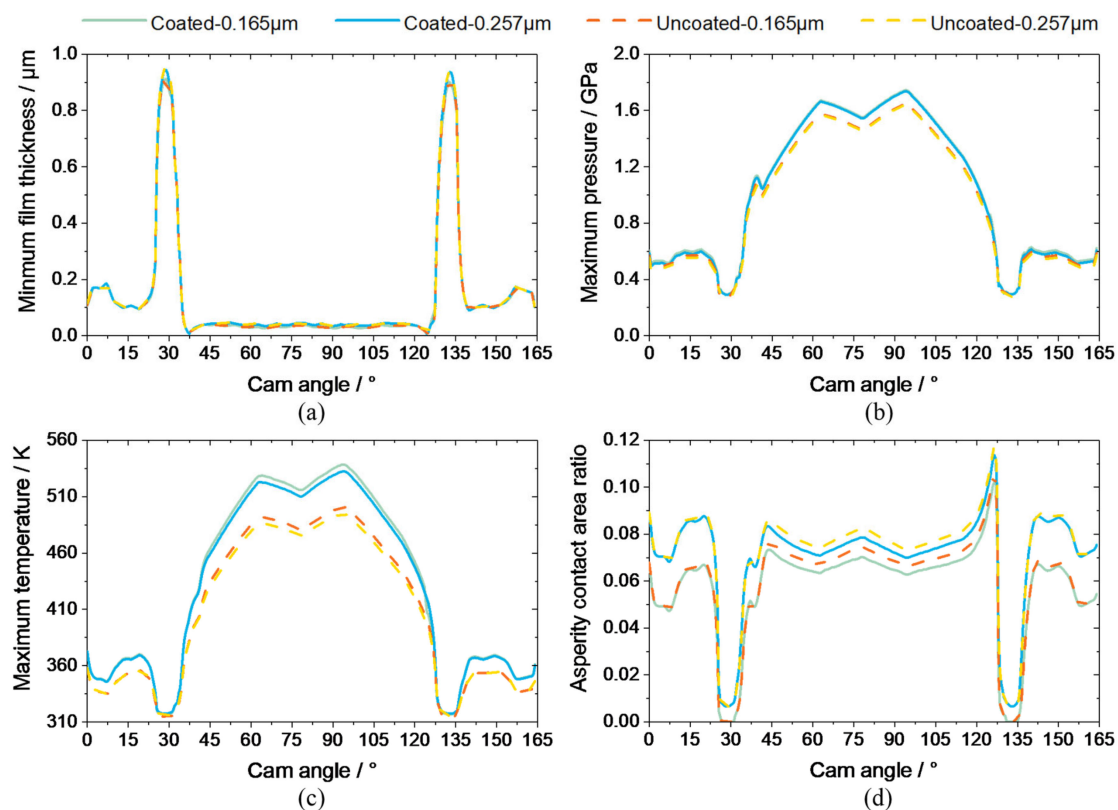

Figure 11. Variations of the lubrication state during a cam cycle under the heavy load: (**a**) the minimum film thickness, (**b**) the maximum film pressure, (**c**) the maximum temperature of the lubricant, and (**d**) the asperity contact area ratio.
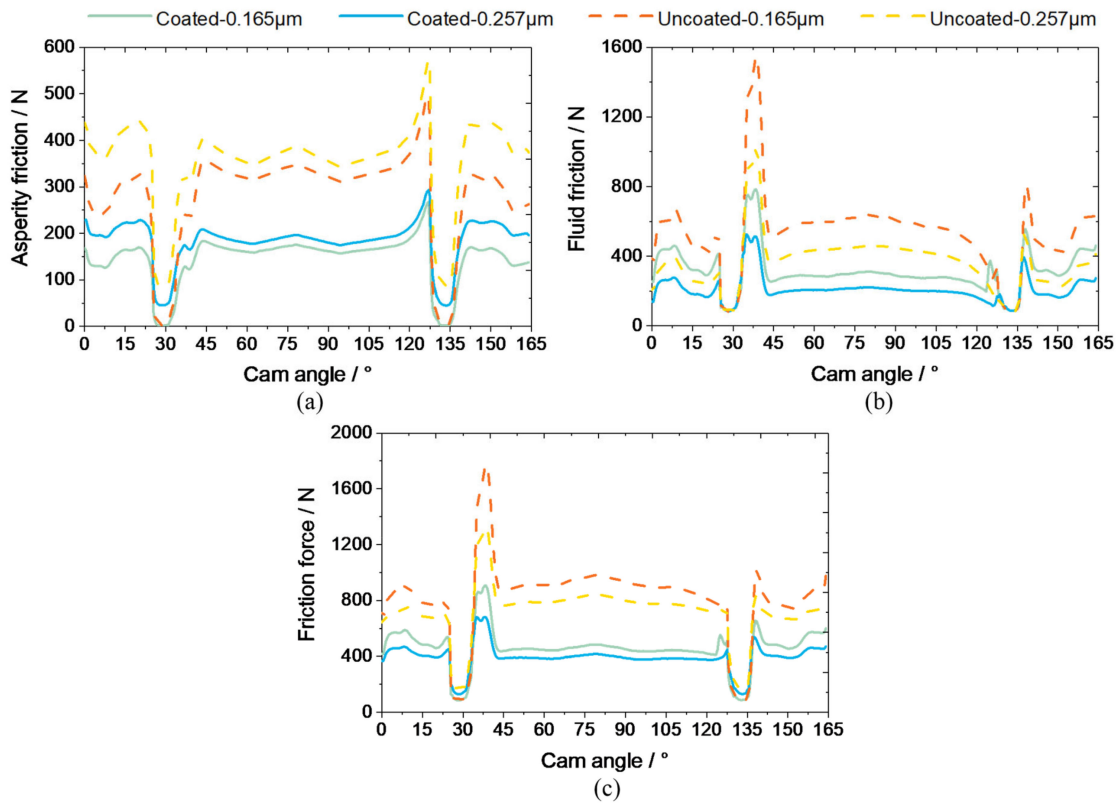
Figure 12. Frictional variations during a cam cycle under the heavy load: (**a**) asperity contact friction, (**b**) fluid friction, and (**c**) total friction.
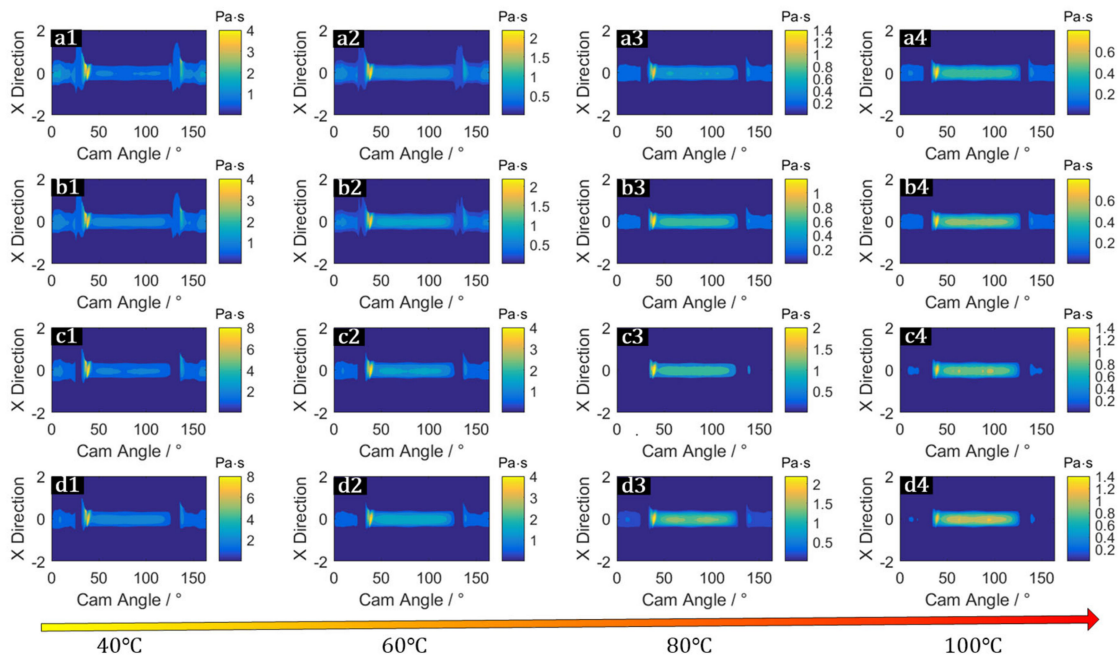

Figure 13. The lubricant viscosity distributions at various ambient temperatures during a cam cycle under the heavy load: (**a1**)–(**a4**) coated surfaces with 0.165 μm roughness, (**b1**)–(**b4**) coated surfaces with 0.257 μm roughness, (**c1**)–(**c4**) uncoated surfaces with 0.165 μm roughness, and (**d1**)–(**d4**) uncoated surfaces with 0.257 μm roughness.
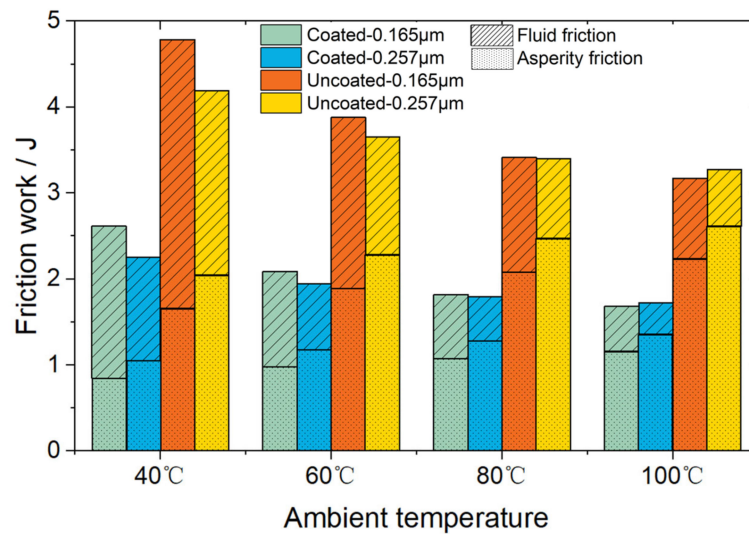
Figure 14. The friction work for different surface conditions at various ambient temperatures in a cam cycle under the heavy load.

In the cases under the heavy load, the friction work in the cam/tappet conjunction with DLC coatings during a whole cam cycle is significantly reduced by up to 45% (Figure 14), compared with the uncoated cases. Consistent with the normal-load condition, as the ambient temperature increases, the fluid friction consumption shrinks continuously, while the asperity friction consumption manifests an expanding trend. The total friction consumption, which is lower at a higher ambient temperature, shows an opposite behaviour with the normal-load cases. This is because the fluid friction consumption accounts for a large proportion in these cases, and it is highly susceptible to the increasing ambient temperature and will decline significantly. Therefore, although the asperity friction consumption will increase to a certain extent, the total friction loss will decrease with the increasing ambient temperature. However, at high ambient temperature phase, the decrease of total friction consumption becomes minor and, predictably, it will start to increase as asperity friction gradually dominates at further higher ambient temperature. It is noteworthy that when the surface roughness increases from 0.165 μm to 0.257 μm at mild ambient temperature, the total friction consumption declines. The applied load is borne more by the asperities for rougher surfaces, resulting in lower hydrodynamic pressure (Figure 11b). Therefore, the viscosity and fluid friction, as well as total friction consumption, will decrease accordingly. However, when the ambient temperature is raised to 100 C, the situation is reversed due to the dominant asperity contact.

Under the heavy load, the wear condition (Figure 15) is similar to the cases in the last section, where DLC coatings show superior anti-wear characteristics with a greatly reduced wear volume. Also, the wear volume presents a positive correlation with the ambient temperature and surface roughness. However, under the heavy load the wear volume is more than twice that under the normal load, and it is predictable that the wear durability will be much shorter accordingly. It is noteworthy that under the heavy load for cam/tappet conjunctions, the asperity contact ratio will inevitably increase substantially. At the cam angle of 124.5 in particular, the asperity contact area ratio exceeds 10% (Figure 11), which is noticeably higher than others. It may be triggered by the zero-entrainment velocity associating with a relatively low lubricant viscosity (Figure 13). However, in the presence of coatings, the friction force and the wear loss of the interacting surfaces are greatly reduced. From this point of view, DLC coatings can also depress the risk of surface failures in friction pairs under heavy loads, such as scuffing.
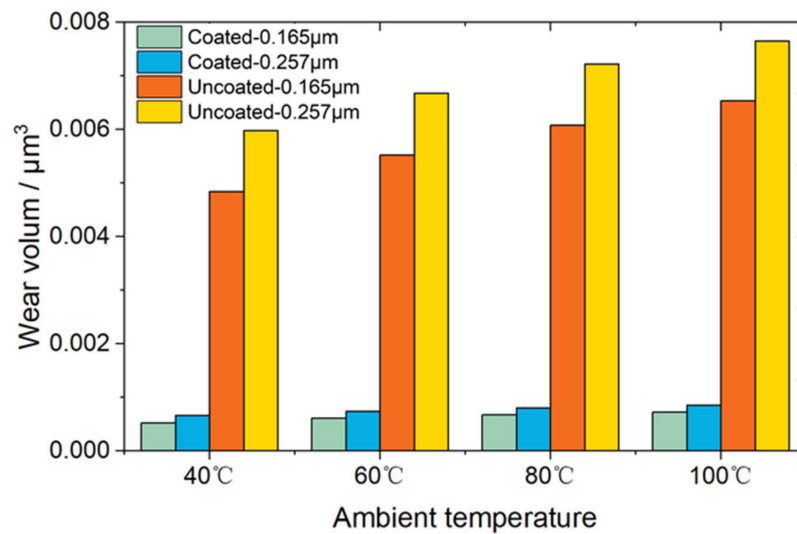
Figure 15. The wear volume for different surface conditions at various ambient temperatures in a cam cycle under the heavy load.

4. Conclusions

More than 75% of the automotive market will still rely on ICEs by 2040 in their traditional role or as a part of a hybrid power train, and coating technology will play a key role in efficiency improvement and emission reduction. A comprehensive multi-physics analytical model of the cam/tappet pairs is developed in this paper, integrating the mechanical, thermal and tribological properties of the DLC coating. The friction coefficient, thermal and load conditions, and surface topography of the DLC coating, which are essential to its practical performance, are investigated. Moreover, considering the more and more severe operating conditions of modern engines, a much heavier-load condition for cam/tappet pairs is discussed. The results can be concluded as follows:

1. The anti-friction effect of coatings is mainly reflected in two aspects. On the one hand, the fluid friction for the coated surface is reduced due to its low thermal inertia, which services as a thermal barrier and results in high lubricant temperature and low shear force. Moreover, the asperity contact friction for the coated surface is also lower owing to its favourable friction coefficient, despite a slightly higher asperity contact.
2. The friction loss during a cam cycle of the coated cam/tappet is noticeably decreased by almost 40%. With the rising ambient temperature, the friction loss increases gradually, where the fluid friction consumption shrinks continuously, while the asperity friction consumption manifests an expanding trend.
3. The wear volume of the coated surface is substantially lower than that of the uncoated, which can be attributed to its high hardness and low wear coefficient. Besides, higher ambient temperature and roughness will result in more severe wear volume.
4. The friction reduction and wear-resistance effect of coatings on cam/tappet pairs under a much heavier load are still valid, and a reduced friction loss up to 45% is achieved in the coated cases. However, the total friction consumption is decreased when the ambient temperature rises from 40 C to 100 C. The wear volume is more than twice that under the normal load, and thus it is predictable that the wear durability will be much shorter.

Author Contributions: Conceptualization, Y.C.; Data curation, B.L.; Formal analysis, B.L.; Funding acquisition, X.M.; Investigation, B.L. and R.Z.; Methodology, B.L., R.Z., and Y.C.; Software, B.L., R.L., and Y.C.; Supervision, X.M. All authors have read and agreed to the published version of the manuscript.

Conflicts of Interest: The authors declare no conflict of interest.

Nomenclature

T_0	Ambient temperature (K)
c	Specific heat of lubricant (J/(kg·K))
$c_{a,b}$, $c_{ac,bc}$	Specific heat of substrates and coatings (J/(kg·K))
d	Clearance between the rough surfaces (μm)
D	Influence coefficient
E_s, E_c	Modulus of elasticity for substrates and coatings (GPa)
f, f_{visco}, f_{asp}	Total, lubricant viscous, and asperity contact friction (N)
h	Film thickness (m)
h_{wear}	Wear depth (m)
H	Hardness (GPa)
j_θ	geometrical acceleration (m)
k	Thermal conductivity of lubricant W/(m K)
$k_{a,b}$, $k_{ac,bc}$	Thermal conductivity of substrates and coatings W/(m·K)
K_W	Wear coefficient
L	Cm thickness (m)
p	Film pressure (Pa)
p_{asp}	Asperity contact pressure (Pa)
R_0	Base circle radius of cam (m)
R_C	Equivalent contact radius (m)
s	Cam lift (m)
s_{ku}	Kurtosis
s_{sk}	Skewness
S	Slide distance (m)
t	Time (s)
T	Lubricant temperature (K)
u, w	Velocities of the control volumes in x and z directions (m/s)
u_a, u_b	Velocities of the cam and tappet (m/s)
u_s	Entrainment velocity (m/s)
v	Elastic deformation of surfaces (m)
v_s, v_c	Poisson's ratio for substrates and coatings
w_f	Friction work (J)
W	Applied load (N/m)
x	Coordinate in rolling direction
x_s, x_e	Leading and trailing edges
z	Coordinate in film thickness direction
α	Thermal expansion coefficient, (K^{-1})
β	Arithmetic mean asperity curvature (μm^{-1})
δ	Root mean square height (μm)
η	Lubricant viscosity (Pa·s)
η_0	Initial lubricant viscosity (Pa·s)
η_a	Density of asperities (μm^{-2})
μ_{asp}	friction coefficient of the dry contact surface
ρ	Lubricant density (kg/m^3)
ρ_0	Initial lubricant density (kg/m^3)
$\rho_{a,b}$, ρ_c	Substrates and coatings density (kg/m^3)
σ	Root mean square height (μm)
σ_c,	Composite roughness (μm)
τ	Viscous shear force (Pa)
ϕ_x, ϕ_c, ϕ_s, ϕ_f, ϕ_{fs}, ϕ_{fp}	Flow factors
ω	Angular velocity of the cam (rad/s)

Appendix A

For the evaluation of surface topography, the standard roughness parameters, Ra and Rq, are widely used. Ra and Rq of surface 2 are larger than those of surface1, which means the former is relatively rougher than the latter (Figure 4). However, these two parameters cannot describe the topography sufficiently. It was shown how two completely different surfaces can show similar, or even the same, values of the standard roughness parameters and vice versa [48]. According to the height distribution of asperities, rough surfaces can be categorized into the Gaussian and non-Gaussian surfaces. Rough surfaces are mostly non-Gaussian in nature [49], including these two measured surfaces. In order to quantify the non-Gaussian aspect of rough surfaces, additional roughness parameters, such as skewness (s_{sk}; Equation (A1)) and kurtosis (s_{ku}; Equation (A2)), are necessary.

$$s_{sk} = \frac{\int_{-\infty}^{\infty} \delta^3 \phi(\delta) d\delta}{\sigma^3} \tag{A1}$$

$$s_{ku} = \frac{\int_{-\infty}^{\infty} \delta^4 \phi(\delta) d\delta}{\sigma^4} \tag{A2}$$

Skewness is sensitive to occasional deep valleys or high peaks in the profile because it measures the symmetry of the variation in a profile about its mean line. A symmetrical height distribution is reflected in zero skewness, whereas positive skewness such as turned surfaces have fairly high spikes that protrude above a flatter average. Negative skewness such as porous surfaces have fairly deep valleys in a smoother plateau (Figure A1). The skewnesses of surface 1 and surface 2 (Table 2) are 0.4545 and −1.0278, respectively. It means the roughness spike of surface 1 is rather high, while on the contrary, the roughness valley of surface 2 is relatively deep (Figure 4). In addition, kurtosis describes the probability density sharpness of the profile. Surfaces with relatively few high peaks and low valleys are reflected in a kurtosis of less than 3, whereas a kurtosis value of more than 3 indicates many high peaks and low valleys ([50]; Figure A1). The kurtosises of surface 1 and surface 2 (Table 2) are both more than 3, and the latter (23.0696) is noticeably larger than the former (10.6186), which means surface 2 is much sharper than surface1 (Figure 4).
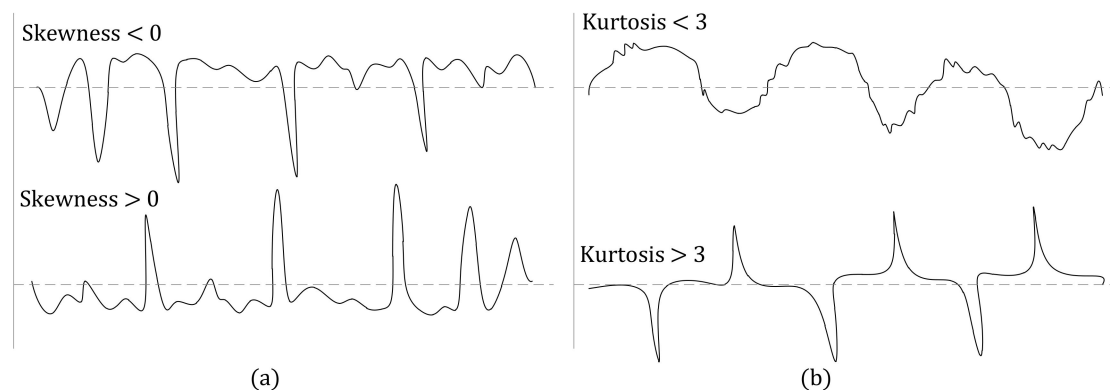

(a)   (b)

Figure A1. Schematic presentation of roughness profiles for (**a**) positive and negative skewness and (**b**) kurtosis lower and higher than 3.

References

1. Kalghatgi, G. Is it really the end of internal combustion engines and petroleum in transport? *Appl. Energy* **2018**, *225*, 965–974. [CrossRef]
2. Dolatabadi, N.; Forder, M.; Morris, N.; Rahmani, R.; Rahnejat, H.; Howell-Smith, S. Influence of advanced cylinder coatings on vehicular fuel economy and emissions in piston compression ring conjunction. *Appl. Energy* **2020**, *259*, 114129. [CrossRef]
3. Serrano, J.R.; Novella, R.; Piqueras, P. Why the Development of Internal Combustion Engines Is Still Necessary to Fight against Global Climate Change from the Perspective of Transportation. *Appl. Sci.* **2019**, *9*, 4597. [CrossRef]
4. Buchal, C.; Karl, H.-D.; Sinn, H.-W. Kohlemotoren, Windmotoren und Dieselmotoren: Was zeigt die CO2-Bilanz? *ifo Schnelldienst.* **2019**, *72*, 40–54.
5. Holmberg, K.; Andersson, P.; Erdemir, A. Global energy consumption due to friction in passenger cars. *Tribol. Int.* **2012**, *47*, 221–234. [CrossRef]

6. Gangopadhyay, A.; McWatt, D.G.; Zdrodowski, R.J.; Simko, S.J.; Matera, S.; Sheffer, K.; Furby, R.S. Valvetrain Friction Reduction through Thin Film Coatings and Polishing. *Tribol. Trans.* **2012**, *55*, 99–108. [CrossRef]

7. Dowson, D.; Taylor, C.M.; Zhu, G. A transient elastohydrodynamic lubrication analysis of a cam and follower. *J. Phys. D Appl. Phys.* **1992**, *25*, A313–A320. [CrossRef]

8. Chong, W.W.F.; Teodorescu, M.; Rahnejat, H. Mixed thermo-elastohydrodynamic cam-tappet power loss in low-speed emission cycles. *Int. J. Engine Res.* **2012**, *15*, 153–164. [CrossRef]

9. Torabi, A.; Akbarzadeh, S.; Salimpour, M.R.; Khonsari, M.M. On the running-in behavior of cam-follower mechanism. *Tribol. Int.* **2018**, *118*, 301–313. [CrossRef]

10. Teodorescu, M.; Taraza, D.; Henein, N.A.; Bryzik, W. Experimental Analysis of Dynamics and Friction in Valve Train Systems. *SAE Tech. Pap. Ser.* **2002**, *2002*, 1027–1037. [CrossRef]

11. Green, D.A.; Lewis, R.; Dwyer-Joyce, R.S. Wear of Valve Train Components Due to Soot Contaminated Lubricant. *SAE Tech. Pap. Ser.* **2006**. [CrossRef]

12. Ohr, R.; Jacoby, B.; Gradowski, M.; Schug, C.; Hilgers, H. Analytical and functional characterization of ultrathin carbon coatings for future magnetic storage devices. *Surf. Coat. Technol.* **2003**, *173*, 111–115. [CrossRef]

13. Kasemo, B. Biological surface science. *Surf. Sci.* **2002**, *500*, 656–677. [CrossRef]

14. Robertson, J. Diamond-like amorphous carbon. *Mater. Sci. Eng. R Rep.* **2002**, *37*, 129–281. [CrossRef]

15. Martin, P. Review of the filtered vacuum arc process and materials deposition. *Thin Solid Films* **2001**, *394*, 1–14. [CrossRef]

16. Kano, M. Super low friction of DLC applied to engine cam follower lubricated with ester-containing oil. *Tribol. Int.* **2006**, *39*, 1682–1685. [CrossRef]

17. Dobrenizki, L.; Tremmel, S.; Wartzack, S.; Hoffmann, D.C.; Brögelmann, T.; Bobzin, K.; Bagcivan, N.; Musayev, Y.; Hosenfeldt, T. Efficiency improvement in automobile bucket tappet/camshaft contacts by DLC coatings – Influence of engine oil, temperature and camshaft speed. *Surf. Coatings Technol.* **2016**, *308*, 360–373. [CrossRef]

18. Habchi, W. A numerical model for the solution of thermal elastohydrodynamic lubrication in coated circular contacts. *Tribol. Int.* **2014**, *73*, 57–68. [CrossRef]

19. Habchi, W. Influence of thermo-mechanical properties of coatings on friction in elastohydrodynamic lubricated contacts. *Tribol. Int.* **2015**, *90*, 113–122. [CrossRef]

20. Bobzin, K.; Brögelmann, T.; Stahl, K.; Michaelis, K.; Mayer, J.; Hinterstoißer, M. Friction reduction of highly-loaded rolling-sliding contacts by surface modifications under elasto-hydrodynamic lubrication. *Wear* **2015**, *328*, 217–228. [CrossRef]

21. Yu, C.; Meng, X.; Xie, Y. Numerical simulation of the effects of coating on thermal elastohydrodynamic lubrication in cam/tappet contact. *Proc. Inst. Mech. Eng. Part J J. Eng. Tribol.* **2016**, *231*, 221–239. [CrossRef]

22. Marian, M.; Weikert, T.; Tremmel, S. On Friction Reduction by Surface Modifications in the TEHL Cam/Tappet-Contact-Experimental and Numerical Studies. *Coatings* **2019**, *9*, 843. [CrossRef]

23. Hauert, R. An overview on the tribological behavior of diamond-like carbon in technical and medical applications. *Tribol. Int.* **2004**, *37*, 991–1003. [CrossRef]

24. Yoshida, Y.; Kunitsugu, S. Friction wear characteristics of diamond-like carbon coatings in oils containing molybdenum dialkyldithiocarbamate additive. *Wear* **2018**, *414*, 118–125. [CrossRef]

25. Steiner, L.; Bouvier, V.; May, U.; Hegadekatte, V.; Huber, N. Modelling of unlubricated oscillating sliding wear of DLC-coatings considering surface topography, oxidation and graphitisation. *Wear* **2010**, *268*, 1184–1194. [CrossRef]

26. Gangopadhyay, A.; Sinha, K.; Uy, D.; McWatt, D.G.; Zdrodowski, R.J.; Simko, S.J. Friction, Wear, and Surface Film Formation Characteristics of Diamond-Like Carbon Thin Coating in Valvetrain Application. *Tribol. Trans.* **2010**, *54*, 104–114. [CrossRef]

27. Patir, N.; Cheng, H.S. An Average Flow Model for Determining Effects of Three-Dimensional Roughness on Partial Hydrodynamic Lubrication. *J. Lubr. Technol.* **1978**, *100*, 12–17. [CrossRef]

28. Patir, N.; Cheng, H.S. Application of Average Flow Model to Lubrication Between Rough Sliding Surfaces. *J. Lubr. Technol.* **1979**, *101*, 220–229. [CrossRef]

29. Roelands, C.J.A.; Winer, W.O.; Wright, W.A. Correlational Aspects of the Viscosity-Temperature-Pressure Relationship of Lubricating Oils (Dr In dissertation at Technical University of Delft, 1966). *J. Lubr. Technol.* **1971**, *93*, 209–210. [CrossRef]

30. Dowson, D.; Higginson, G.R. *Elasto-Hydrodynamic Lubrication: International Series on Materials Science and Technology*; Elsevier: Amsterdam, The Netherlands, 2014.

31. Habchi, W.; Eyheramendy, D.; Vergne, P.; Morales-Espejel, G. Stabilized fully-coupled finite elements for elastohydrodynamic lubrication problems. *Adv. Eng. Softw.* **2012**, *46*, 4–18. [CrossRef]

32. Chu, L.-M.; Chen, C.-Y.; Tee, C.-K.; Chen, Q.-D.; Li, W.-L. Elastohydrodynamic Lubrication Analysis for Transversely Isotropic Coating Layer. *J. Tribol.* **2014**, *136*, 031502. [CrossRef]

33. Greenwood, J.A.; Williamson, J.B.P. Contact of nominally flat surfaces. *Proc. R. Soc. Lond. Ser. A Math. Phys. Sci.* **1966**, *295*, 300–319.

34. Greenwood, J.A.; Tripp, J.H. The Contact of Two Nominally Flat Rough Surfaces. In Proceedings of the Institution of Mechanical Engineers; SAGE Publications: London, UK, 1970; Volume 185, pp. 625–633.

35. Chang, W.-R.; Etsion, I.; Bogy, D.B. An Elastic-Plastic Model for the Contact of Rough Surfaces. *J. Tribol.* **1987**, *109*, 257–263. [CrossRef]

36. Kogut, L.; Etsion, I. A Finite Element Based Elastic-Plastic Model for the Contact of Rough Surfaces. *Tribol. Trans.* **2003**, *46*, 383–390. [CrossRef]

37. Tian, X.; Bhushan, B. A Numerical Three-Dimensional Model for the Contact of Rough Surfaces by Variational Principle. *J. Tribol.* **1996**, *118*, 33–42. [CrossRef]

38. Liu, Z.; Meng, X.; Wen, C.; Yu, S.; Zhou, Z. On the oil-gas-solid mixed bearing between compression ring and cylinder liner under starved lubrication and high boundary pressures. *Tribol. Int.* **2019**, *140*, 105869. [CrossRef]

39. Ai, X.; Sawamiphakdi, K. Solving Elastic Contact Between Rough Surfaces as an Unconstrained Strain Energy Minimization by Using CGM and FFT Techniques. *J. Tribol.* **1999**, *121*, 639–647. [CrossRef]

40. Yang, P.; Qu, S.; Kaneta, M.; Nishikawa, H. Formation of Steady Dimples in Point TEHL Contacts. *J. Tribol.* **2000**, *123*, 42–49. [CrossRef]

41. Masjedi, M.; Khonsari, M.M. Theoretical and experimental investigation of traction coefficient in line-contact EHL of rough surfaces. *Tribol. Int.* **2014**, *70*, 179–189. [CrossRef]

42. Wang, J.; Yang, P. A Numerical Analysis for TEHL of Eccentric-Tappet Pair Subjected to Transient Load. *J. Tribol.* **2003**, *125*, 770–779. [CrossRef]

43. Kim, N.-W.; Kim, K.-W. Effects of sliding velocity and ambient temperature on the friction and wear of a boundary-lubricated, multi-layered DLC coating. *Wear* **2014**, *315*, 95–102. [CrossRef]

44. Meng, X.; Gu, C.; Zhang, D. Modeling the wear process of the ring/liner conjunction considering the evaluation of asperity height distribution. *Tribol. Int.* **2017**, *112*, 20–32. [CrossRef]

45. Archard, J.F. Contact and Rubbing of Flat Surfaces. *J. Appl. Phys.* **1953**, *24*, 981. [CrossRef]

46. Zabala, B.; Igartua, A.; Fernández, X.; Priestner, C.; Ofner, H.; Knaus, O.; Abramczuk, M.; Tribotte, P.; Girot, F.; Roman, E.; et al. Friction and wear of a piston ring/cylinder liner at the top dead centre: Experimental study and modelling. *Tribol. Int.* **2017**, *106*, 23–33. [CrossRef]

47. Teodorescu, M.; Rahnejat, H.; Gohar, R.; Dowson, D. Harmonic decomposition analysis of contact mechanics of bonded layered elastic solids. *Appl. Math. Model.* **2009**, *33*, 467–485. [CrossRef]

48. Esen, H.; Inalli, M. ANN and ANFIS models for performance evaluation of a vertical ground source heat pump system. *Expert Syst. Appl.* **2010**, *37*, 8134–8147. [CrossRef]

49. Gu, C.; Meng, X.; Wang, S.; Ding, X. Research on Mixed Lubrication Problems of the Non-Gaussian Rough Textured Surface with the Influence of Stochastic Roughness in Consideration. *J. Tribol.* **2019**, *141*, 1–36. [CrossRef]

50. Ye, X.; Tse, Z.T.; Tang, G.; Li, X.; Song, G. Retraction notice to: "Effect of electropulsing treatment on microstructure and mechanical properties of cold-rolled pure titanium strips" [Journal of Materials Processing Technology, Volume 222, August 2015, Pages 27-32]. *J. Mater. Process. Technol.* **2019**, *268*, 223. [CrossRef]